

# 000 001 002 003 004 005 PARTNER-AWARE HIERARCHICAL SKILL DISCOVERY 006 FOR ROBUST HUMAN-AI COLLABORATION 007 008 009

010 **Anonymous authors**  
011  
012  
013  
014  
015  
016  
017  
018  
019  
020  
021  
022  
023  
024  
025  
026  
027  
028  
029  
030  
031  
032  
033  
034  
035  
036  
037  
038  
039  
040  
041  
042  
043  
044  
045  
046  
047  
048  
049  
050  
051  
052  
053

Paper under double-blind review

## ABSTRACT

Multi-agent collaboration, especially in human-AI (HAI) teaming, requires agents that can adapt to novel partners with diverse and dynamic behaviors. Conventional Deep Hierarchical Reinforcement Learning (DHRL) methods focus on agent-centric rewards and overlook partner behavior, leading to shortcut learning, where skills exploit spurious information instead of adapting to partners' dynamic behaviors. This limitation undermines agents' ability to adapt and coordinate effectively with novel partners. We introduce Partner-Aware Skill Discovery (PASD), a DHRL framework learning skills conditioned on partner behavior. PASD introduces a contrastive intrinsic reward to capture patterns emerging from partner interactions, aligning skill representations across similar partners while maintaining discriminability across diverse strategies. By structuring the skill space based on partner interactions, this approach mitigates shortcut learning and promotes behavioral consistency, enabling robust and adaptive coordination. **We conduct extensive evaluations in Overcooked-AI across three complementary settings: (1) a diverse self-play partner population spanning a wide range of skill levels and play styles, (2) human proxy partners trained from real human–human trajectories, and (3) a controlled human-subject study with 25 participants.** PASD consistently outperforms existing population-based and hierarchical baselines, demonstrating transferable skill learning that generalizes across a wide range of partner behaviors. Analysis of learned skill representations shows that PASD adapts effectively to diverse partner behaviors, highlighting its robustness in HAI collaboration.

## 1 INTRODUCTION

Developing intelligent agents that can coordinate effectively with humans and other novel partners has long been a central challenge in multi-agent reinforcement learning (MARL) (Klein et al., 2004; Alami et al., 2006; Bard et al., 2020). Unlike adversarial settings (Ye et al., 2020), where success is measured by outperforming an opponent, collaboration is far more challenging as it requires adapting to novel partners with diverse and often unpredictable behaviors (Hu et al., 2020). Early approaches relied on behavior cloning (BC) from human–human interaction data, but these methods are costly, time-consuming, and struggle to capture the diversity of real-world behaviors (Carroll et al., 2019). **Furthermore, even in fully observable environments, partner behaviors are not fully predictable from a single state. Differences in timing, hesitation, movement rhythms, and style preferences unfold over sequences of actions, requiring temporal modeling to capture and adapt to these patterns. Conditioning on the current state is insufficient to avoid behavioral interference or forgetting of previously learned coordination strategies.** More recently, hierarchical reinforcement learning (HRL) has advanced collaboration by decomposing complex tasks into reusable skills, enabling more structured exploration and improved coordination (Eysenbach et al., 2019; Loo et al., 2023). HRL provides a framework for structuring agent behavior through temporally extended actions, or 'skills', which can capture reusable patterns of behavior. By learning a set of diverse and reusable skills, agents can explore more efficiently and adapt their behavior in complex environments.

However, standard skill discovery methods remain largely agent-centric, optimizing for diversity without accounting for partner influence. Consequently, the learned skills may support individual performance but are insufficient for robust coordination with diverse partners. We argue that this limitation arises from the agent-centric nature of reward optimization. Existing approaches maximise expected returns from the agent's perspective, often ignoring the influence of the partner on

054 cooperative dynamics. This misalignment leads to *shortcut learning* (Wei et al., 2023), where agents  
 055 exploit spurious correlations in the environment rather than capturing information relevant for part-  
 056 ner interactions. As a result, agents develop behaviors that prioritize their own action diversity but  
 057 fail to generalize coordination across novel partners.

058 Prior skill discovery methods in HRL often maximize mutual information (MI) between skills and  
 059 observational states as a proxy for behavioral diversity Gregor et al. (2016); Eysenbach et al. (2019).  
 060 While this encourages the agent to develop distinguishable behaviors, the objective is bounded by  
 061 the entropy of skills and does not ensure sensitivity to partner behavior. As a result, these approaches  
 062 often learn simple and static skills with limited adaptability, leading to poor state coverage and weak  
 063 coordination, as highlighted in recent studies (Campos et al., 2020; Jiang et al., 2022). Moreover,  
 064 tractable variational estimators of MI (Eysenbach et al., 2019), typically implemented with neural  
 065 networks optimized via cross-entropy or related objectives, are prone to shortcut learning . In prac-  
 066 tice, they often capture spurious correlations in state features rather than the interaction patterns  
 067 relevant for effective collaboration Wei et al. (2023).

068 We introduce Partner-Aware Skill Discovery (PASD), an HRL approach for learning skills that adapt  
 069 to diverse collaborator behaviors. PASD maximizes a variational lower bound on MI between skills  
 070 and sub-trajectories, encouraging representations that are consistent and reproducible across part-  
 071 ner interactions. This is achieved via a contrastive objective that ensures skill representations are  
 072 discriminative across heterogeneous partners while remaining consistent for partners with similar  
 073 behaviors. By capturing patterns shaped by partner behavior rather than agent-centric correlations,  
 074 PASD mitigates shortcut learning and produces skills that generalize across partners, supporting  
 075 effective partner-adaptive coordination.

076 In summary, our work makes the following key contributions. First, we introduce PASD, a DHRL  
 077 framework that enables robust human-AI coordination through skill representations conditioned on  
 078 partner behavior. Second, a novel contrastive intrinsic reward is proposed and incorporated into  
 079 PASD to encourage consistency in skill representations across similar partners by capturing shared  
 080 patterns from parallel rollouts while maintaining discriminability across diverse partner behaviors.  
 081 This intrinsic reward, derived from contrastive learning, encourages behavioral diversity across di-  
 082 verse partners, mitigating shortcut learning caused by spurious state information, and directly lever-  
 083 aging partner-relevant information from the observational space. **We further emphasize that PASD**  
 084 **leverages HRL to mitigate forgetting by learning separate latent skills and captures temporal pat-**  
 085 **terns of partner behavior, enabling robust adaptation to diverse human-like coordination styles even**  
 086 **in fully observable environments. Finally, we extensively evaluate PASD in the Overcooked-AI en-**  
 087 **vironment, partnering the agent with a diverse self-play population spanning multiple skill levels**  
 088 **and play styles, as well as with human-proxy models trained from human-human demonstrations.**  
 089 **In addition, a controlled human-subject study with real human participants further shows that PASD**  
 090 **yields significantly higher joint rewards than existing approaches, demonstrating that PASD learns**  
 091 **transferable skills that generalize effectively across a wide range of partners, enabling robust and**  
 092 **adaptive human-AI coordination.**

## 093 2 RELATED WORK

094 Recent work has explored building agents that can coordinate with human partners Carroll et al.  
 095 (2019); Hao et al. (2024). Carroll et al. Carroll et al. (2019) introduced the *Overcooked-AI* environ-  
 096 ment and trained PPO agents with human proxy models from human gameplay. While improving  
 097 robustness, this requires extensive and costly human data. Hao et al. Hao et al. (2024) introduce  
 098 intrinsic rewards to encourage agents to explore states that yield sparse rewards when coordinat-  
 099 ing with human proxy models. Strouse et al. Strouse et al. (2021) propose Fictitious Co-Play (FCP),  
 100 generating a pool of self-play policies and past versions to train adaptive agents without human data.  
 101 Some works further improve partner heterogeneity using entropy-based objectives during training  
 102 (Lupu et al., 2021; Garnelo et al., 2021; Zhao et al., 2023; Loo et al., 2023). Hidden-utility Self-Play  
 103 HSP (Yu et al., 2023) extends FCP by modeling human biases as hidden reward functions, generating  
 104 a diverse policies to train adaptive agents that can cooperate with unseen humans with preferences  
 105 deviating from environment rewards. **Jha et al. Jha et al. (2025) propose Cross-Environment Cooper-**  
 106 **ation (CEC), which trains agents across a distribution of environments to acquire general cooperative**  
 107 **skills, enabling zero-shot coordination with novel partners. While effective for generalization across**

108 tasks, CEC does not explicitly model partner-adaptive skill discovery within a single environment,  
 109 which is the focus of our method. While these methods focus on learning a single-level agent pol-  
 110 icy, effective human-AI coordination requires reasoning over temporally extended behaviors and  
 111 adapting to partners with diverse and evolving strategies.

112 HRL provides a framework for reasoning over temporally extended behaviors, making it well-suited  
 113 for multi-agent and human-AI coordination. By learning policies at multiple temporal levels (Sutton  
 114 et al., 1999; Flet-Berliac, 2019; Pateria et al., 2021), HRL captures high-level strategic planning and  
 115 low-level execution. Classical approaches such as options (Bacon et al., 2017; Eysenbach et al.,  
 116 2019) and feudal learning (Vezhnevets et al., 2017) illustrate temporal hierarchy benefits, extended  
 117 to cooperative multi-agent settings in recent work (Loo et al., 2023; Yang et al., 2023a). Methods like  
 118 DIAYN (Eysenbach et al., 2019) encourage diverse behaviors using intrinsic rewards maximizing  
 119 MI between skills and states/actions. However, these agent-centric approaches are prone to shortcut  
 120 learning, capturing spurious patterns instead of partner-relevant behaviors. Hierarchical Population  
 121 Training (HIPT) (Loo et al., 2023) adapts HRL to human-AI coordination by shaping the high-  
 122 level policy via influence-based intrinsic rewards but trains the low-level policy only on extrinsic  
 123 rewards, risking skill collapse. Our approach introduces a novel intrinsic reward to mitigate shortcut  
 124 learning, ensuring behavioral consistency across similar partners while remaining discriminative to  
 125 diverse strategies, supporting adaptive human-AI coordination

### 3 PRELIMINARIES

126 We consider a multi-agent setting in which two agents collaborate to complete shared tasks, with  
 127 the framework naturally extending to settings involving more agents. One agent is controlled by  
 128 a learning policy  $\pi_\theta(\cdot | s_t)$ , while the other is governed by a partner policy  $\pi^p(\cdot | s_t)$ , sampled  
 129 uniformly from a population of pretrained partners  $\mathcal{D}_p$  at the start of each episode. The objec-  
 130 tive is to train  $\pi_\theta(\cdot | s_t)$  to achieve high returns when paired with novel partners drawn from a  
 131 separate evaluation distribution  $\mathcal{D}'_p$ . The environment is modeled as a two-player Markov game  
 132  $\mathcal{M} = (\mathcal{S}, \mathcal{A}, \mathcal{A}^p, \mathcal{P}, r, \gamma, \rho_0)$ , where  $\mathcal{S}$  is the state space,  $\mathcal{A}$  and  $\mathcal{A}^p$  are the action spaces of the  
 133 learning agent and the partner,  $\mathcal{P}$  is the transition kernel,  $r : \mathcal{S} \times \mathcal{A} \times \mathcal{A}^p \rightarrow \mathbb{R}$  is the shared team  
 134 reward,  $\gamma \in (0, 1)$  is the discount factor, and  $\rho_0$  is the initial state distribution. At each timestep  $t$ ,  
 135 the learning agent selects an action  $a_t \sim \pi_\theta(\cdot | s_t)$ , while the partner executes  $a_t^p \sim \pi^p(\cdot | s_t)$ , and  
 136 the next state is drawn from  $s_{t+1} \sim \mathcal{P}(s_{t+1} | s_t, a_t, a_t^p)$ .  
 137

138 From the perspective of the learning agent, the effective dynamics marginalize over both the part-  
 139 ner's stochasticity and the population distribution:

$$\mathcal{P}_{\mathcal{D}_p}(s' | s, a) = \mathbb{E}_{\pi^p \sim \mathcal{D}_p} \mathbb{E}_{a^p \sim \pi^p(\cdot | s)} [\mathcal{P}(s' | s, a, a^p)].$$

140 This formulation emphasizes that the agent must learn a policy that is robust to variations in partner  
 141 behavior while maximizing expected returns over the population of collaborators. For a given partner  
 142  $\pi^p$ , the return is

$$J(\pi_\theta | \pi^p) = \mathbb{E} \left[ \sum_{t=0}^{\infty} \gamma^t r(s_t, a_t, a_t^p) \right]. \quad (1)$$

143 To encourage robustness to novel partners, the learning objective is the expected return over the  
 144 partner population:

$$J(\pi_\theta) = \mathbb{E}_{\pi^p \sim \mathcal{D}_p} [J(\pi_\theta | \pi^p)]. \quad (2)$$

145 **Hierarchical reinforcement learning:** In collaborative multi-agent environments, effective coor-  
 146 dination requires reasoning over temporally extended behaviors and adapting to partners with diverse  
 147 and dynamically changing strategies. To capture these aspects, we model the learning agent using  
 148 a hierarchical policy inspired by the options framework Sutton et al. (1999). Formally, we consider  
 149 DHRL setup with a high-level manager  $\pi_{hi}(z | s)$  and a low-level controller  $\pi_{lo}(a | s, z)$ . The  
 150 high-level manager selects latent skills  $z \in \mathcal{Z}$ , which guide temporally extended behaviors executed  
 151 by the low-level controller. Each skill  $z_k$  is executed over a segment from  $t_k$  to  $t_{k+1} - 1$ , producing  
 152 cumulative segment reward:  
 153

$$\mathcal{R}^Z(s_{t_k}, z_k) = \sum_{t=t_k}^{t_{k+1}-1} \gamma^{t-t_k} r(s_t, a_t, a_t^p), \quad z_k \sim \pi_{hi}(\cdot | s_{t_k}), \quad a_t \sim \pi_{lo}(\cdot | s_t, z_k), \quad (3)$$

162 where  $a_t^p$  denotes the partner’s action at time  $t$  and  $\gamma \in [0, 1]$  is a discount factor. The high-level  
163 objective is the expected return over all skill segments:

$$165 \quad J_{hi}(\pi_{hi}, \pi_{lo} \mid \pi^p) = \mathbb{E} \left[ \sum_{k=0}^{K-1} \gamma^{t_k} \mathcal{R}^Z(s_{t_k}, z_k) \right]. \quad (4)$$

166 Skill execution is controlled by a stochastic termination function  $\beta(z, s)$ , which determines whether  
167 the current skill continues or a new skill should be selected. This allows the manager to adaptively  
168 update skills at irregular intervals  $T_{hi}$  based on the evolving collaborative context.

169 Within each skill segment, the low-level controller  $\pi_{lo}(a \mid s, z)$  outputs primitive actions conditioned  
170 on the current state and the active skill. The low-level policy is trained to reliably realize the intended  
171 skill, producing sequences of actions that induce state transitions  $s \rightarrow s'$  through the environment  
172 dynamics. Formally, the low-level objective can be expressed as:

$$175 \quad J_{lo}(\pi_{lo} \mid z, \pi^p) = \mathbb{E} \left[ \sum_{t=t_k}^{t_{k+1}-1} \gamma^{t-t_k} r(s_t, a_t, a_t^p) \right], \quad (5)$$

176 where the expectation is conditioned on the currently active skill  $z_k$ . The high-level manager,  
177 low-level controller, and termination function together define the joint hierarchical policy  $\pi =$   
178  $(\pi_{hi}, \pi_{lo}, \beta)$ , which is optimized end-to-end via proximal policy optimization (PPO) algorithm  
179 (Schulman et al., 2017) to maximize both high-level and low-level objectives.

## 182 4 METHOD

### 184 4.1 MOTIVATION

185 While the high-level and low-level objectives in 4 and 5 focus on maximizing extrinsic team rewards,  
186 optimizing only for these objectives often leads to skill collapse, where all skills converge to similar  
187 behaviors. Each skill independently maximizes cumulative reward without explicit constraints  
188 promoting discriminability, which can result in a single skill dominating entire episodes. Under  
189 such conditions, the termination function  $\beta(z, s)$  cannot effectively differentiate among skills, and  
190 the hierarchical policy loses expressive power. Prior works Eysenbach et al. (2019); Gregor et al.  
191 (2016) have addressed skill collapse by introducing intrinsic objectives that maximize the mutual  
192 information (MI) between skills and states,  $I(Z; S) = H(Z) - H(Z \mid S)$ , thereby encouraging skills  
193 to induce distinguishable state distributions. These approaches typically separate skill discovery  
194 and high-level optimization into two phases: skills are first discovered by mapping them to diverse  
195 states, and then the high-level policy is optimized with extrinsic reward on downstream tasks.

196 However, in collaborative multi-agent environments, the next state is determined jointly by the agent  
197 and the partner policy,  $s_{t+1} \sim \mathcal{P}(s_{t+1} \mid s_t, a_t, a_t^p)$ , so the state distribution induced by a skill  $z$   
198 depends not only on the agent policy  $\pi$  but also on the partner policy  $\pi^p$ .

199 **Assumption 1:** The skill space is lower-dimensional than the joint state space, i.e.,  $H(Z) <$   
200  $H(S)$ ,  $s \sim \rho^{\pi, \pi^p}(s)$ . This reflects the fact that each skill typically corresponds to a sub-trajectory  
201 of the high-dimensional state space, allowing distinct behaviors to be captured as separate skills.

202 Under Assumption 1, maximizing  $I(Z; S)$  is limited by the low dimensionality of the skill space.  
203 Since  $H(Z)$  is fixed, the agent can achieve the maximum MI even by producing only minor, agent-  
204 centric variations that capture very little meaningful information about the partner-conditioned dy-  
205 namics. For instance, consider two policies  $\pi_1$  and  $\pi_2$  that interact with the same partner  $\pi^p$ . Sup-  
206 pose  $\pi_2$  explores the state space more broadly than  $\pi_1$ , which is reflected by:  $H_{\rho^{\pi_1, \pi^p}}(S) <$   
207  $H_{\rho^{\pi_2, \pi^p}}(S)$ . However, since  $Z$  has fixed entropy  $H(Z)$ , maximizing the MI still yields

$$210 \quad \max I(Z; S)_{\pi_1} = \max I(Z; S)_{\pi_2} = H(Z), \quad (6)$$

211 meaning that  $I(Z; S)$  alone does not distinguish policies with different exploration capacities. Thus,  
212  $I(Z; S)$  provides no extra information to prefer policies that better coordinate with the partner.

213 Furthermore, variational approximations of  $H(Z \mid S)$  typically rely on neural networks (NN) trained  
214 via cross-entropy (CE) loss, which is well known to be biased toward spurious information in fea-  
215 ture space Wei et al. (2023). As a result, the agent can increase  $I(Z; S)$  through local, repeatable

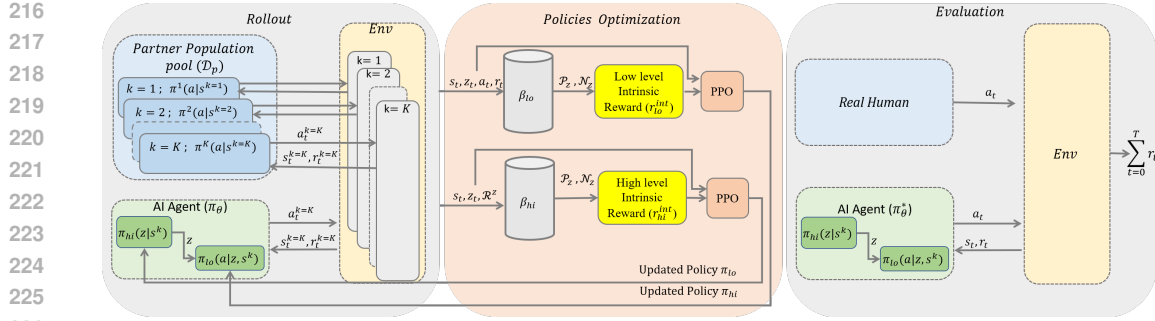


Figure 1: **Overview of PASD training and evaluation.** **Left:** PASD is trained with  $K$  parallel rollouts, each paired with a different partner sampled from the partner pool  $\mathcal{D}_p$ . After every episode, high-level and low-level trajectories are stored in buffers  $\beta_h$  and  $\beta_l$ . These trajectories are used to form *positive* pairs  $\mathcal{P}_z$  (same skill across different partners) and *negative* pairs  $\mathcal{N}_z$  (different skills), enabling computation of the contrastive intrinsic rewards in Eq. 13. **Right:** The optimized policies  $\pi_{hi}$  and  $\pi_{lo}$  are evaluated with real human partners to measure collaborative performance.

perturbations that are largely agent-centric and do not improve coordination. Formally, maximizing  $I(Z; S)$  does not prevent large conditional divergences,  $\text{KL}(\pi_{hi}(\cdot | s_1) \| \pi_{hi}(\cdot | s_2))$ ,  $s_1 \approx s_2$ , for states corresponding to similar partner behaviour, implying that high entropy does not necessarily ensure alignment with  $\pi^p$ . These observations motivate a more structured objective that conditions skill discovery on partner-relevant information and encourages skills to be meaningfully distinct. In particular, skill embeddings should capture partner behaviors, ensuring that discovered skills reflect collaborative interactions rather than agent-only perturbations.

## 4.2 PARTNER-ADAPTIVE SKILLS DISCOVERY

In collaborative settings such as Overcooked Carroll et al. (2019), the behavior induced by a skill is shaped jointly by the agent and its partner. The same high-level skill may lead to different state transitions depending on whether the partner is fast, slow, or prioritizes different tasks. Thus, discovering meaningful skills requires capturing how a skill behaves across diverse partner policies, not just how the agent behaves in isolation. The objective in this section is to construct skill representations that remain consistent when interacting with behaviorally similar partners while remaining discriminative across different skills, ensuring that behaviorally distinct skills induce distinguishable interaction patterns. Figure 1 illustrates the overall PASD framework, showing both the training setup with partner interactions and the evaluation process with human partners. To capture partner influence as a skill discriminability measure, consider collecting  $K$  parallel rollouts under the joint dynamics of the skill-conditioned agent and the partner:

$$\tau^{(k)} \sim \rho^{\pi(\cdot | s, z), \pi^p \sim D^p}(\tau), \quad k = 1, \dots, K, \quad (7)$$

where  $\rho^{\pi, \pi^p}(\tau)$  denotes the trajectory distribution induced by the agent-partner interaction. Each rollout is segmented into  $M$  sub-trajectories of length  $L$ :

$$\tau^{(k,j)} = \{s_{t_j}, a_{t_j}, \dots, s_{t_j+L}\}, \quad j = 1, \dots, M, \quad (8)$$

and representative states are sampled from each sub-trajectory,  $s^{(k,j)} \sim \tau^{(k,j)}$ .

**Assumption 2:** We assume that distinct sub-trajectory views of the same skill encode a consistent partner-adaptive strategy, independent of which partner  $\pi^p \sim \mathcal{D}_p$  is sampled, up to stochastic noise. In other words, for any two views  $(k_1, j_1) \neq (k_2, j_2)$ , the additional information about the skill identity provided by one view given the other is negligible:

$$I(S^{(k_1, j_1)}; Z | S^{(k_2, j_2)}) \approx 0, \quad \text{or equivalently} \quad S^{(k_1, j_1)} \perp\!\!\!\perp Z | S^{(k_2, j_2)}. \quad (9)$$

Intuitively, once one view is observed, other views add little new information about the skill identity, reflecting reproducible partner-conditioned behavior across the partner population despite stochastic variations in trajectories. Under Assumption 2, the MI between sub-trajectory states can be used

270 to discover useful partner-conditioned skills i.e., skills that are both distinct with diverse partner  
 271 behavior and consistent across partners showing similar behavior:  
 272

$$273 I(S^{(k_1, j_1)}; S^{(k_2, j_2)}) = I(S^{(k_1, j_1)}; S^{(k_2, j_2)}; Z) + I(S^{(k_1, j_1)}; S^{(k_2, j_2)} | Z, \pi^p), \quad (10)$$

275 where the first term captures *skill-discriminative information*, and the second term captures *intra-*  
 276 *skill consistency* across similar partner behaviors.

277 Direct computation of the MI objective in Equation (10) is generally intractable. Following prior  
 278 work van den Oord et al. (2018), we approximate it using a tractable lower bound implemented  
 279 via a contrastive objective over learned state embeddings  $\phi(s)$ . This approximation preserves the  
 280 discriminability of skills across heterogeneous partner behaviors while maintaining consistency for  
 281 similar partner behaviors, and can be directly interpreted as an intrinsic reward signal to shape skill  
 282 representations.

283 For each skill  $z$ , let the index set of its sub-trajectory views be  $\mathcal{P}_z \equiv \{(k, j) : \tau^{(k, j)}\}$ . Positive pairs  
 284 are sampled from two distinct views  $(k_1, j_1), (k_2, j_2) \in \mathcal{P}_z$ , while negative samples are drawn from  
 285 views of other skills,  $\mathcal{N}_z \equiv \bigcup_{z' \neq z} \mathcal{P}_{z'}$ . We approximate MI using an InfoNCE-style contrastive  
 286 loss (Guo et al., 2022) over normalized embeddings  $\phi(s)$ , i.e.,  $\|\phi(s)\|_2 = 1$ , so that similarities are  
 287 measured on the unit hypersphere. For an anchor state  $s$ , with positive set  $\mathcal{P}_z$  and negative set  $\mathcal{N}_z$ ,  
 288 per-anchor InfoNCE loss is:

$$290 \mathcal{L}_{\text{InfoNCE}} = -\frac{1}{|\mathcal{P}_z|} \sum_{s^+ \in \mathcal{P}_z} \log \frac{\exp(\text{sim}(\phi(s), \phi(s^+))/\tau)}{\sum_{s' \in \mathcal{P}_z \cup \mathcal{N}_z} \exp(\text{sim}(\phi(s), \phi(s'))/\tau)}, \quad (11)$$

293 where  $\text{sim}(\cdot, \cdot)$  is the cosine similarity and  $\tau > 0$  is a temperature parameter.

294 By the InfoNCE bound van den Oord et al. (2018), maximizing this reward increases a variational  
 295 lower bound on the MI between the skill variable  $Z$  and the state embeddings  $\phi(S)$ :

$$297 I(\phi(S); Z) \geq \log(N) - \mathcal{L}_{\text{InfoNCE}}, \quad (12)$$

299 where  $N = |\mathcal{N}_z|$  is the number of negatives. The tightness of this approximation depends on the  
 300 number of negative samples  $N$  and the total number of skills  $|\mathcal{Z}|$ . Larger numbers of negatives and  
 301 more diverse skills increase the quality of the lower bound, providing a stronger learning signal.  
 302 This formulation ensures that the learned embeddings  $\phi(s)$  capture both skill distinctiveness and  
 303 consistency across partner behaviors. The InfoNCE objective is applied over carefully constructed  
 304 positive and negative pairs. Positive pairs consist of sub-trajectories generated by the same skill  
 305 interacting with different partners, which encourages embeddings to be consistent across partner be-  
 306 haviors. Negative pairs come from sub-trajectories of other skills, ensuring embeddings are distinct  
 307 for behaviorally different skills. By maximizing InfoNCE, the learned embeddings  $\phi(s)$  capture pat-  
 308 terns that are reproducible and conditioned on the partner, rather than arbitrary agent-centric state  
 309 differences. This ensures that the discovered skills reflect meaningful partner-adaptive dynamics.

### 310 4.3 CONTRASTIVE INTRINSIC REWARD

312 To facilitate the discovery of partner-conditioned skills, we derive an intrinsic reward by leveraging  
 313 the InfoNCE objective. Specifically, the per-anchor InfoNCE probability, which measures similarity  
 314 between states corresponding to the same skill relative to other skills, can be directly used as an  
 315 intrinsic reward signal for both high-level and low-level policies.

316 For each anchor state  $s \in \mathcal{P}_z$ , we compute a contrastive intrinsic reward as

$$318 r^{\text{int}}(s) = \frac{1}{|\mathcal{P}_z|} \sum_{s^+ \in \mathcal{P}_z} \frac{\exp(\text{sim}(\phi(s), \phi(s^+))/\tau)}{\sum_{s' \in \mathcal{P}_z \cup \mathcal{N}_z} \exp(\text{sim}(\phi(s), \phi(s'))/\tau)}, \quad (13)$$

321 where  $\phi(s)$  denotes a normalized state embedding ( $\|\phi(s)\|_2 = 1$ ),  $\text{sim}(\cdot, \cdot)$  is the cosine similarity,  
 322 and  $\tau > 0$  is a temperature parameter. This intrinsic reward encourages the policy to select skills that  
 323 are both discriminative across heterogeneous partner behaviors and consistent across sub-trajectory  
 324 views corresponding to partners with similar behaviors.



Figure 2: The five standard Overcooked layouts (left to right): Cramped Room, Asymmetric Advantages, Coordination Ring, Counter Circuit and Forced Coordination.

#### 4.4 OVERALL TRAINING OBJECTIVE

To effectively learn partner-adaptive skills, we integrate the intrinsic reward defined in Equation (13) with the extrinsic environment reward in both high-level and low-level objectives mentioned in Equations (4 and 5). For the high-level manager, the intrinsic reward is accumulated and normalized over each skill segment  $[t_k, t_{k+1} - 1]$ :

$$\tilde{\mathcal{R}}^Z(s_{t_k}, z_k) = \frac{1}{t_{k+1} - t_k} \sum_{t=t_k}^{t_{k+1}-1} \left( (1 - \lambda) r(s_t, a_t, a_t^p) + \lambda r^{\text{int}}(s_t) \right), \quad (14)$$

where  $\lambda \in [0, 1]$  controls the relative weighting of intrinsic and extrinsic rewards. The corresponding high-level objective is

$$\tilde{J}_{hi} = \mathbb{E} \left[ \sum_{k=0}^{K-1} \gamma^{t_k} \tilde{\mathcal{R}}^Z(s_{t_k}, z_k) \right]. \quad (15)$$

In the early phase of training, the intrinsic reward dominates, promoting exploration of diverse skill patterns and capturing variations in partner behaviors across different rollouts. As training progresses, the influence of the extrinsic reward gradually increases, guiding the high-level manager to refine skill selection toward maximizing task returns while maintaining consistency and discriminability across partner-conditioned interactions. For the low-level controller, the intrinsic reward is applied at each timestep:

$$\tilde{J}_{lo} = \mathbb{E} \left[ \sum_{t=t_k}^{t_{k+1}-1} \gamma^{t-t_k} \left( r(s_t, a_t, a_t^p) + \lambda r^{\text{int}}(s_t) \right) \right]. \quad (16)$$

Initially, the intrinsic reward drives the low-level policy to produce diverse and disentangled action distributions for each skill, capturing the variability in partner behaviors across different rollouts. As training progresses, the extrinsic reward gradually increases in influence, aligning these action distributions with task objectives while preserving the discriminability and consistency of behaviors for partners with similar tendencies. Both high-level and low-level objectives are optimized with the PPO algorithm, using the rewards defined in Equations 15 and 16. Detailed pseudocode describing the rollout procedure and the policy optimization steps of PASD is provided in Appendix A.

## 5 EXPERIMENTS

### 5.1 EXPERIMENTAL DETAILS

**Environment:** Following existing works (Strouse et al., 2021; Loo et al., 2023; Yu et al., 2023; Yang et al., 2023b), we adopt the Overcooked-AI Carroll et al. (2019) as our testbed. Overcooked-AI is a two-player cooperative benchmark derived from the Overcooked game Games (2016), in which agents collaboratively complete a soup preparation task. Agents must pick onions, place them in the pot, wait for the soup to cook, and then deliver the completed soup to the serving station, with each successful delivery yielding a reward of +20. The goal is to maximize team reward within

378 Table 1: Total mean reward (Mean  $\pm$  Std) across three versions of each evaluation partner (early,  
 379 intermediate, final checkpoint) and both starting positions.

Method	Cramped Room	Asym. Adv.	Coord. Ring	Counter Circuit	Forced Coord.
FCP	$137.7 \pm 1.0$	$90.6 \pm 1.0$	$83.9 \pm 5.9$	$51.3 \pm 5.0$	$36.7 \pm 14.4$
DIAYN	$33.8 \pm 6.4$	$1.5 \pm 0.7$	$22.5 \pm 6.3$	$1.2 \pm 1.0$	$1.3 \pm 0.0$
HiPT	$117.9 \pm 4.4$	$86.2 \pm 0.9$	$96.0 \pm 1.3$	$38.1 \pm 5.3$	$35.6 \pm 13.0$
PASD	<b><math>165.8 \pm 10.0</math></b>	<b><math>145.8 \pm 9.6</math></b>	<b><math>101.3 \pm 8.5</math></b>	<b><math>57.37 \pm 2.9</math></b>	<b><math>46.87 \pm 12.3</math></b>

388 a fixed episode horizon. We evaluate across five standard layouts, *Cramped Room*, *Asymmetric*  
 389 *Advantages*, *Coordination Ring*, *Forced Coordination*, and *Counter Circuit*, illustrated in Figure 2.  
 390 These layouts present diverse coordination challenges and collectively provide a widely adopted  
 391 benchmark for studying partner-adaptive behaviors. **Overcooked-AI is fully observable, making it a**  
 392 **suitable testbed where coordination challenges arise solely from partner behavior rather than partial**  
 393 **observability Yu et al. (2023); Yang et al. (2023b)**. For a detailed discussion of layout-specific  
 394 demands, see Appendix B.

395 **Diverse Self-Play Partner Population:** For effective coordination with novel partners and hu-  
 396 mans, the AI agent is trained with a diverse partner population, where each partner has a unique  
 397 play style and skill level. Following prior work Strouse et al. (2021); Lupu et al. (2021); Loo et al.  
 398 (2023), we construct a heterogeneous policy pool. The pool consists of 16 agents trained via self-  
 399 play with PPO, varying in play style and skill level. Diverse play styles are encouraged using a  
 400 negative Jensen–Shannon Divergence (Loo et al., 2023), and varying skill levels are included via  
 401 intermediate checkpoints (Strouse et al., 2021). During training, a partner is uniformly sampled  
 402 from the heterogeneous population each episode. For evaluation with novel AI partners, a separate  
 403 disjoint population of the same size is trained using the same procedure.

404 **Baselines** We compare PASD against standard baselines including FCP (Strouse et al., 2021),  
 405 DIAYN (Eysenbach et al., 2019), and HiPT (Loo et al., 2023). Each method is trained and evaluated  
 406 with the identical set of diverse partner populations introduced earlier. FCP trains the adaptive policy  
 407 directly with PPO, whereas DIAYN, HiPT, and PASD adopt HRL where high-level and low-level  
 408 policies are jointly optimized via the option-critic framework (Sutton et al., 1999). DIAYN uses a  
 409 two-stage process where skills are first acquired through intrinsic rewards and then fine-tuned for  
 410 task performance, while HiPT and PASD train both levels of the hierarchy in parallel.

411 **Implementation Details:** We train all methods for  $10^7$  steps using 30 parallel rollouts with a  
 412 horizon length of 400. For PASD, the weighting coefficient  $\lambda$  is linearly annealed from 1.0 to 0.05  
 413 during training. Both low-level and high-level policies share a backbone network that consists of  
 414 three convolution layers, two fully connected layers, and a recurrent LSTM layer. The network is  
 415 then split into separate heads for low-level action and value prediction, and for high-level skill and  
 416 value estimation. The discrete skill variable  $z$  is set to dimension 6 for all layouts except *Forced*  
 417 *Coordination*, where it is set to 5. Additional hyperparameter details are provided in Appendix D.

## 418 5.2 RESULTS

419 We organize our results into three evaluation categories based on partner type. First, the agent is  
 420 paired with a diverse self-play population (Section 5.1) to test adaptation to novel AI behaviors.  
 421 Second, we evaluate with human proxy models trained via behavior cloning on human–human tra-  
 422 jectories, providing a closer approximation of human collaboration. Third, we validate performance  
 423 through a controlled human-subject study to assess real human-AI coordination.

424 **Evaluation with Self-Play Partner Population:** We first evaluate all methods using the hetero-  
 425 geneous partner population, organized into three sets, early-stage, intermediate, and fully trained  
 426 policies, covering a spectrum of partner proficiency from beginner to advanced. This population  
 427 serves as a practical proxy for varied human collaborative behaviors (Strouse et al., 2021; Yu et al.,  
 428 2023). For each set, we report the mean episodic return across all partners and starting positions,

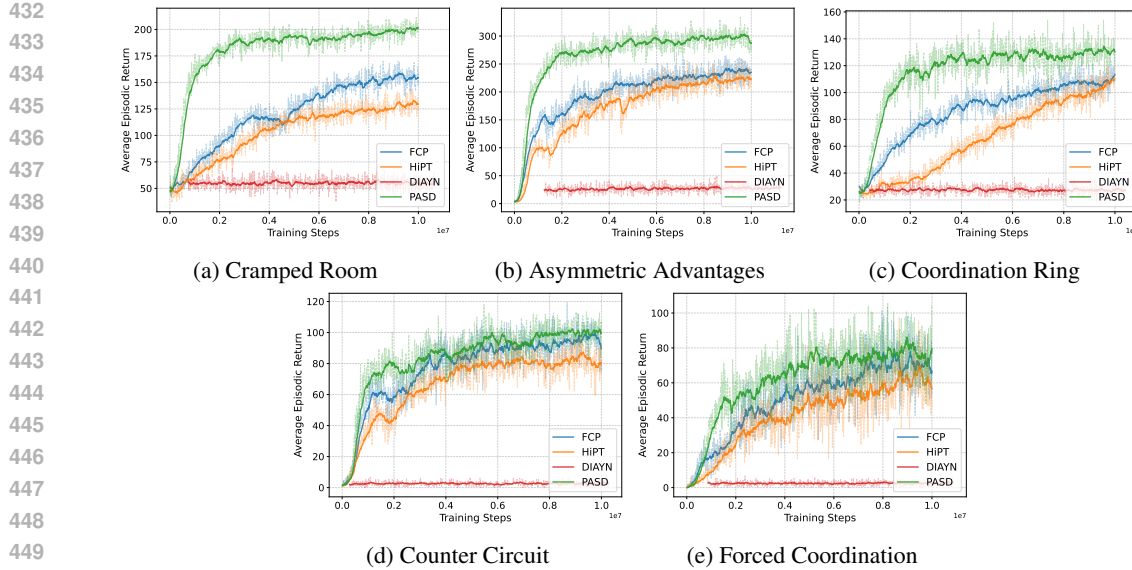


Figure 3: Average episodic return during training across 30 parallel rollout environments.

Table 2: Total mean reward across different layouts when paired with a Behaviour Cloning (BC) partner.

Method	Cramped Room	Asym. Adv.	Coord. Ring	Counter Circuit	Forced Coord.
FCP	118.75	80.00	79.38	38.13	30.75
DIAYN	40.00	0.00	26.25	1.25	6.30
HiPT	93.13	66.25	77.50	35.00	25.20
PASD	<b>150.00</b>	<b>112.50</b>	<b>105.63</b>	<b>44.38</b>	<b>43.8</b>

with overall performance summarized as mean  $\pm$  standard deviation across the three sets (Table 1). Performance varies with layout difficulty. DIAYN performs poorly due to spurious variations disrupting skill learning. HiPT and FCP perform better but remain sensitive to redundant state information. In contrast, PASD robustly captures partner-relevant behaviors, avoids spurious variations, and achieves the highest returns across all layouts. Figures 3a–3e show average returns over 30 rollouts, illustrating that PASD converges faster and maintains stable performance across diverse partner behaviors and coordination challenges.

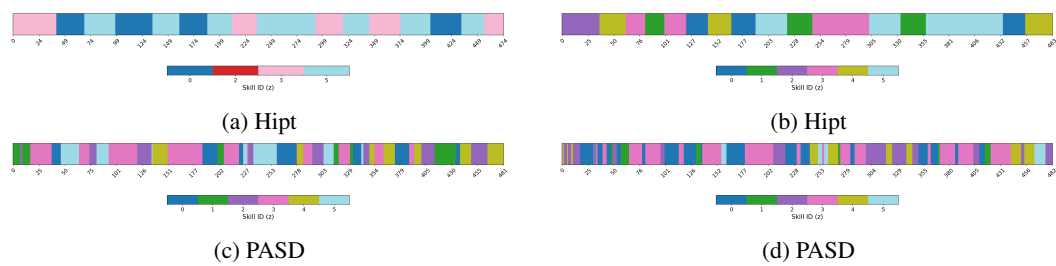
**Evaluation with Human Proxy Partner:** We now turn our attention to evaluating all methods with a human proxy partner trained on real human data. This proxy is obtained via behavior cloning on publicly available human–human trajectories collected by Carroll et al. (Carroll et al., 2019). Following the same procedure, the model is trained to imitate human demonstrations and used as a fixed partner during evaluation, providing a realistic approximation of human behavior under controlled conditions. Results are reported in Table 2. Performance of all methods slightly drops compared to evaluation with the self-play population, as behavior cloning with limited human data can produce policies that favor a dominant action and occasionally stall without random perturbations, as noted in (Carroll et al., 2019). Despite these challenges, PASD continues to achieve the highest returns, highlighting its ability to generalize effectively to previously unseen human-like partners.

**Human Subject Study: Real Human–AI Collaboration Evaluation** To evaluate PASD in real human–AI collaboration, we conducted a controlled human-subject study following Carroll et al. (2019). We recruited 25 participants via Amazon Mechanical Turk (AMT), each completing two episodes of 20 minutes: one paired with HiPT and one with PASD. The order of methods was randomized to mitigate ordering effects. To limit session duration and reduce participant fatigue, only HiPT and PASD were included, omitting other baselines. Participants who did not complete

486  
487  
488  
489 Table 3: Total mean reward (Mean  $\pm$  Standard Deviation) achieved by human participants when  
490 paired with HiPT and PASD across different Overcooked layouts.  
491  
492

Method	Cramped Room	Asym. Adv.	Coord. Ring	Counter Circuit	Forced Coord.
HiPT	80.00 $\pm$ 16.34	136.36 $\pm$ 20.36	46.0 $\pm$ 12.36	40.00 $\pm$ 15.81	20 $\pm$ 0.0
PASD	118.18 $\pm$ 12.68	198.18 $\pm$ 19.41	60.0 $\pm$ 08.92	62.5 $\pm$ 10.95	35.0 $\pm$ 10.00

493  
494 both episodes were excluded, leaving 19 valid participants. Trajectories and rewards were recorded  
495 for all layouts and evaluation partners. Table 3 reports the mean  $\pm$  standard deviation of total reward  
496 across conditions. Across all layouts, PASD consistently achieved higher joint rewards with human  
497 partners than HiPT, improving human-AI collaboration by 22–47%, demonstrating that partner-  
498 conditioned skill discovery meaningfully enhances real-world coordination. The full experimental  
499 setup is available at our anonymized GitHub repository <sup>1</sup>.



500  
501  
502  
503  
504 Figure 4: Skill activation over the trajectory for HiPT and PASD in Cramped Room (Left) and  
505 Coordination Ring (Right) layouts. Each colored block represents a distinct skill selected by the  
506 agent at a given timestep.  
507  
508

513  
514 **Qualitative Analysis of Skill Disentanglement** To illustrate how PASD (blue agent) adapts to  
515 human behaviors, we conducted controlled sessions in the Cramped Room and Coordination Ring  
516 layouts. Each session lasted 80 seconds ( 482 steps), simulating diverse gameplay for the human  
517 agent. In the Cramped Room, humans demonstrated varying preferences, e.g., picking plates from  
518 different sides or collecting soup in distinct sequences. The AI agent had to adapt by selecting the  
519 appropriate skill to minimize collisions and coordinate effectively. Similarly, in Coordination Ring,  
520 humans coordinated either clockwise or counter-clockwise, requiring agent adaptation to match the  
521 chosen pattern. Figure 4 visualizes skill usage over entire trajectories for both HiPT and PASD.  
522 PASD demonstrates distinct and stable skill activation corresponding to different human behaviors,  
523 producing sequences of atomic actions aligned with intended behavior patterns. In contrast, HiPT  
524 switches skills infrequently, often after completing entire tasks, indicating skill collapse or shortcut  
525 learning, as it fails to capture behavior-specific action patterns. Full trajectory frames and animated  
526 visualizations are available in the GitHub repository <sup>1</sup>, illustrating how PASD adaptively selects  
527 skills to accommodate diverse human strategies throughout the episode. These results highlight  
528 PASD’s ability to disentangle skills across behavioral modes, enhancing human-AI coordination.  
529 Quantitative analysis of skill variability and adaptation across partners is provided in Appendix C

## 6 CONCLUSION

530  
531 This work presents PASD, a DHRL approach that introduces an intrinsic reward designed to enable  
532 effective human-AI coordination. The reward leverages a contrastive objective that encourages skill  
533 representations to be consistent across similar partners while remaining discriminative across diverse  
534 partner strategies. By capturing patterns shaped by partner behaviors, PASD promotes behavioral  
535 consistency and robustness, naturally mitigating shortcut learning that can arise from spurious in-  
536 formation in the state space. Our experiments in Overcooked-AI demonstrate that PASD learns  
537 transferable skills that generalize across a wide range of partners, providing a foundation for more  
538 adaptive and efficient collaborative agents.  
539

<sup>1</sup> <https://anonymous.4open.science/r/pasd-22495/>

540 REFERENCES  
541

542 Rachid Alami, Aurélie Clodic, Vincent Montreuil, Emrah Akin Sisbot, and R. Chatila. To-  
543 ward human-aware robot task planning. In *AAAI Spring Symposium: To Boldly Go Where No*  
544 *Human-Robot Team Has Gone Before*, 2006. URL <https://api.semanticscholar.org/CorpusID:2769694>.

545

546 Pierre-Luc Bacon, Jean Harb, and Doina Precup. The option-critic architecture. In *Proceedings of*  
547 *the AAAI conference on artificial intelligence*, volume 31, 2017.

548

549 Nolan Bard, Jakob N Foerster, Sarath Chandar, Neil Burch, Marc Lanctot, H Francis Song, Emilio  
550 Parisotto, Vincent Dumoulin, Subhodeep Moitra, Edward Hughes, et al. The hanabi challenge: A  
551 new frontier for ai research. *Artificial Intelligence*, 280:103216, 2020.

552

553 Víctor Campos, Alexander Trott, Caiming Xiong, Richard Socher, Xavier Giró-i Nieto, and Jordi  
554 Torres. Explore, discover and learn: Unsupervised discovery of state-covering skills. In *Inter-*  
555 *national conference on machine learning*, pp. 1317–1327. PMLR, 2020.

556

557 Micah Carroll, Rohin Shah, Mark K Ho, Tom Griffiths, Sanjit Seshia, Pieter Abbeel, and Anca  
558 Dragan. On the utility of learning about humans for human-ai coordination. *Advances in neural*  
559 *information processing systems*, 32, 2019.

560

561 Benjamin Eysenbach, Julian Ibarz, Abhishek Gupta, and Sergey Levine. Diversity is all you need:  
562 Learning skills without a reward function. In *7th International Conference on Learning Repre-*  
563 *sentations, ICLR 2019*, 2019.

564

565 Yannis Flet-Berliac. The promise of hierarchical reinforcement learning. *The Gradient*, 9, 2019.

566

567 Ghost Town Games. Overcooked. [https://store.steampowered.com/app/448510/](https://store.steampowered.com/app/448510/Overcooked/)  
568 Overcooked/, 2016. Video game.

569

570 Marta Garnelo, Wojciech Marian Czarnecki, Siqi Liu, Dhruva Tirumala, Junhyuk Oh, Gauthier  
571 Gidel, Hado van Hasselt, and David Balduzzi. Pick your battles: Interaction graphs as population-  
572 level objectives for strategic diversity. In *Proceedings of the 20th International Conference on*  
573 *Autonomous Agents and MultiAgent Systems*, pp. 1501–1503, 2021.

574

575 Karol Gregor, Danilo Jimenez Rezende, and Daan Wierstra. Variational intrinsic con-  
576 trol. *ArXiv*, abs/1611.07507, 2016. URL <https://api.semanticscholar.org/CorpusID:2918187>.

577

578 Yiduo Guo, Bing Liu, and Dongyan Zhao. Online continual learning through mutual information  
579 maximization. In *International conference on machine learning*, pp. 8109–8126. PMLR, 2022.

580

581 Xin Hao, Bahareh Nakisa, Mohammad Naim Rastgoo, and Gaoyang Pang. Bcr-drl: Behavior- and  
582 context-aware reward for deep reinforcement learning in human-ai coordination. 2024. URL  
583 <https://api.semanticscholar.org/CorpusID:271874309>.

584

585 Hengyuan Hu, Adam Lerer, Alex Peysakhovich, and Jakob Foerster. “other-play” for zero-shot  
586 coordination. In *International Conference on Machine Learning*, pp. 4399–4410. PMLR, 2020.

587

588 Kunal Jha, Wilka Carvalho, Yancheng Liang, Simon Shaolei Du, Max Kleiman-Weiner, and Natasha  
589 Jaques. Cross-environment cooperation enables zero-shot multi-agent coordination. In *Forty-*  
590 *second International Conference on Machine Learning*, 2025. URL <https://openreview.net/forum?id=zBBYsVGKuB>.

591

592 Zheyuan Jiang, Jingyue Gao, and Jianyu Chen. Unsupervised skill discovery via recurrent skill  
593 training. *Advances in Neural Information Processing Systems*, 35:39034–39046, 2022.

594

595 Gary Klein, David D. Woods, Jeffrey M. Bradshaw, Robert R. Hoffman, and Paul J. Feltovich.  
596 Ten challenges for making automation a “team player” in joint human-agent activity. *IEEE In-*  
597 *tell. Syst.*, 19:91–95, 2004. URL <https://api.semanticscholar.org/CorpusID:27049933>.

594 Yi Loo, Chen Gong, and Malika Meghjani. A hierarchical approach to population training for  
 595 human-ai collaboration. In *IJCAI*, 2023.

596

597 Andrei Lupu, Brandon Cui, Hengyuan Hu, and Jakob Foerster. Trajectory diversity for zero-shot  
 598 coordination. In Marina Meila and Tong Zhang (eds.), *Proceedings of the 38th International  
 599 Conference on Machine Learning*, volume 139 of *Proceedings of Machine Learning Research*, pp.  
 600 7204–7213. PMLR, 18–24 Jul 2021. URL <https://proceedings.mlr.press/v139/lupu21a.html>.

601

602 Shubham Pateria, Budhitama Subagdja, Ah-hwee Tan, and Chai Quek. Hierarchical reinforcement  
 603 learning: A comprehensive survey. *ACM Computing Surveys (CSUR)*, 54(5):1–35, 2021.

604

605 John Schulman, Filip Wolski, Prafulla Dhariwal, Alec Radford, and Oleg Klimov. Proximal policy  
 606 optimization algorithms. *arXiv preprint arXiv:1707.06347*, 2017.

607

608 DJ Strouse, Kevin McKee, Matt Botvinick, Edward Hughes, and Richard Everett. Collaborating  
 609 with humans without human data. *Advances in neural information processing systems*, 34:14502–  
 610 14515, 2021.

611

612 Richard S. Sutton, Doina Precup, and Satinder Singh. Between mdps and semi-mdps: A framework  
 613 for temporal abstraction in reinforcement learning. *Artificial Intelligence*, 112(1):181–211, 1999.  
 614 ISSN 0004-3702. doi: [https://doi.org/10.1016/S0004-3702\(99\)00052-1](https://doi.org/10.1016/S0004-3702(99)00052-1). URL <https://www.sciencedirect.com/science/article/pii/S0004370299000521>.

615

616 Aäron van den Oord, Yazhe Li, and Oriol Vinyals. Representation learning with contrastive predic-  
 617 tive coding. *ArXiv*, abs/1807.03748, 2018. URL <https://api.semanticscholar.org/CorpusID:49670925>.

618

619 Alexander Sasha Vezhnevets, Simon Osindero, Tom Schaul, Nicolas Heess, Max Jaderberg, David  
 620 Silver, and Koray Kavukcuoglu. Feudal networks for hierarchical reinforcement learning. In  
 621 *International conference on machine learning*, pp. 3540–3549. PMLR, 2017.

622

623 Yujie Wei, Jiaxin Ye, Zhizhong Huang, Junping Zhang, and Hongming Shan. Online prototype  
 624 learning for online continual learning. *2023 IEEE/CVF International Conference on Computer  
 625 Vision (ICCV)*, pp. 18718–18728, 2023. URL <https://api.semanticscholar.org/CorpusID:260351482>.

626

627 Mingyu Yang, Yaodong Yang, Zhenbo Lu, Wengang Zhou, and Houqiang Li. Hier-  
 628 archical multi-agent skill discovery. In A. Oh, T. Naumann, A. Globerson,  
 629 K. Saenko, M. Hardt, and S. Levine (eds.), *Advances in Neural Information Process-  
 630 ing Systems*, volume 36, pp. 61759–61776. Curran Associates, Inc., 2023a. URL  
 631 [https://proceedings.neurips.cc/paper\\_files/paper/2023/file/c276c3303c0723c83a43b95a44a1fcfbf-Paper-Conference.pdf](https://proceedings.neurips.cc/paper_files/paper/2023/file/c276c3303c0723c83a43b95a44a1fcfbf-Paper-Conference.pdf).

632

633 Mingyu Yang, Yaodong Yang, Zhenbo Lu, Wengang Zhou, and Houqiang Li. Hierarchical multi-  
 634 agent skill discovery. *Advances in Neural Information Processing Systems*, 36:61759–61776,  
 635 2023b.

636

637 Deheng Ye, Guibin Chen, Wen Zhang, Sheng Chen, Bo Yuan, Bo Liu, Jia Chen, Zhao Liu, Fuhao  
 638 Qiu, Hongsheng Yu, et al. Towards playing full moba games with deep reinforcement learning.  
 639 *Advances in Neural Information Processing Systems*, 33:621–632, 2020.

640

641 Chao Yu, Jiaxuan Gao, Weilin Liu, Botian Xu, Hao Tang, Jiaqi Yang, Yu Wang, and Yi Wu. Learning  
 642 zero-shot cooperation with humans, assuming humans are biased. In *The Eleventh International  
 643 Conference on Learning Representations*, 2023. URL <https://openreview.net/forum?id=TrwE819aJzs>.

644

645 Rui Zhao, Jinming Song, Yufeng Yuan, Haifeng Hu, Yang Gao, Yi Wu, Zhongqian Sun, and Wei  
 646 Yang. Maximum entropy population-based training for zero-shot human-ai coordination. In  
 647 *Proceedings of the AAAI Conference on Artificial Intelligence*, volume 37, pp. 6145–6153, 2023.

648 A PASD – ROLLOUT AND POLICY UPDATE PROCEDURES  
649  
650  
651  
652653 **Algorithm 1** PASD — Rollout and Intrinsic Reward Computation

---

654 1: **Input:** Partner population  $\mathcal{D}_p$ , high-level policy  $\pi_{hi}(z|s)$ , low-level policy  $\pi_{lo}(a|s, z)$   
 655 2: **Parameters:** Intrinsic reward weight  $\lambda$ , rollout horizon  $T$ , skill segment length  $L$   
 656 3: Initialize empty rollout buffers  $\mathcal{B}_{hi}, \mathcal{B}_{lo}$   
 657 4: **for** each parallel rollout  $k = 1, \dots, K$  **do**  
 658   5:   Sample partner policy  $\pi^p \sim \mathcal{D}_p$   
 659   6:   Reset environment  $s_0 \sim \rho_0$   
 660   7:   Initialize  $t \leftarrow 0$   
 661   8:   **while**  $t < T$  **do**  
 662     9:     Sample skill  $z_t \sim \pi_{hi}(z|s_t)$   
 663     10:    **repeat**  
 664       11:    Sample low-level action  $a_t \sim \pi_{lo}(a|s_t, z_t)$   
 665       12:    Sample partner action  $a_t^p \sim \pi^p(a|s_t)$   
 666       13:    Step environment:  $s_{t+1}, r_t \leftarrow \text{EnvStep}(s_t, a_t, a_t^p)$   
 667       14:    Store  $(s_t, z_t, a_t, r_t)$  in low-level buffer  $\mathcal{B}_{lo}$   
 668       15:    Sample termination  $b_t \sim \beta(z_t, s_{t+1})$   
 669       16:     $t \leftarrow t + 1$   
 670     17:    **until** termination  $b_t$  or  $t \geq T$   
 671     18:    Compute high-level segment reward  $R^Z(s_{t_k}, z_t)$  as sum of extrinsic rewards  
 672     19:    Store  $(s_{t_k}, z_t, R^Z)$  in high-level buffer  $\mathcal{B}_{hi}$   
 673   20:   **end while**  
 674   21:   **end for**  
 675 22: Construct positive pairs  $\mathcal{P}_z$  and negative pairs  $\mathcal{N}_z$  from  $\mathcal{B}_{hi}$  for each skill  $z$   
 676 23: Compute contrastive intrinsic rewards  $r^{int}(s)$  using InfoNCE (Eq. 13)  
 677 24: Combine intrinsic and extrinsic rewards using Equations : (14, 15 and 16)  
 678 25: **Output:** High-level buffer  $\mathcal{B}_{hi}$ , low-level buffer  $\mathcal{B}_{lo}$  with combined rewards

---

679  
680  
681682 **Algorithm 2** PASD: Hierarchical Policy Update (High-level, Low-level, Termination)

---

683 1: **Input:** High-level buffer  $\mathcal{B}_{hi}$ , low-level buffer  $\mathcal{B}_{lo}$ , high-level policy  $\pi_{hi}$ , low-level policy  $\pi_{lo}$ ,  
 684   termination policy  $\beta$   
 685 2: **Parameters:** PPO clipping  $\epsilon$ , discount  $\gamma$ , GAE  $\lambda_{GAE}$ , learning rate  $\alpha$   
 686 3: **for** each gradient update iteration **do**  
 687   4:   Compute high-level advantages  $\hat{A}_t^h$  from  $\mathcal{B}_{hi}$  using GAE  
 688   5:   Compute low-level advantages  $\hat{A}_t^l$  from  $\mathcal{B}_{lo}$  using GAE  
 689   6:   Compute termination advantages  $\hat{A}_t^\beta$  from  $\mathcal{B}_{hi}$  or  $\mathcal{B}_{lo}$   
 690   7:   Compute PPO ratio  $r_t^h(\theta) = \frac{\pi_{hi, \theta}(z_t|s_t)}{\pi_{hi, \theta_{old}}(z_t|s_t)}$   
 691   8:   Compute clipped PPO loss with entropy:  $L^h = -\mathbb{E} \left[ \min(r_t^h \hat{A}_t^h, \text{clip}(r_t^h, 1 - \epsilon, 1 + \epsilon) \hat{A}_t^h) \right]$   
 692   9:   Compute PPO ratio  $r_t^l(\theta) = \frac{\pi_{lo, \theta}(a_t|s_t, z_t)}{\pi_{lo, \theta_{old}}(a_t|s_t, z_t)}$   
 693   10:   Compute clipped PPO loss with entropy:  $L^l = -\mathbb{E} \left[ \min(r_t^l \hat{A}_t^l, \text{clip}(r_t^l, 1 - \epsilon, 1 + \epsilon) \hat{A}_t^l) \right]$   
 694   11:   Compute PPO ratio  $r_t^\beta(\theta) = \frac{\beta_\theta(b_t|s_t, z_t)}{\beta_{\theta_{old}}(b_t|s_t, z_t)}$   
 695   12:   Compute clipped PPO loss with entropy:  $L^\beta = -\mathbb{E} \left[ \min(r_t^\beta \hat{A}_t^\beta, \text{clip}(r_t^\beta, 1 - \epsilon, 1 + \epsilon) \hat{A}_t^\beta) \right]$   
 696   13:   Update parameters  $\theta$  of  $\pi_{hi}, \pi_{lo}, \beta$  using  $L^h + L^l + L^\beta$   
 697 14: **end for**  
 698 15: **Return:** Updated policies  $\pi_{hi}, \pi_{lo}, \beta$

---

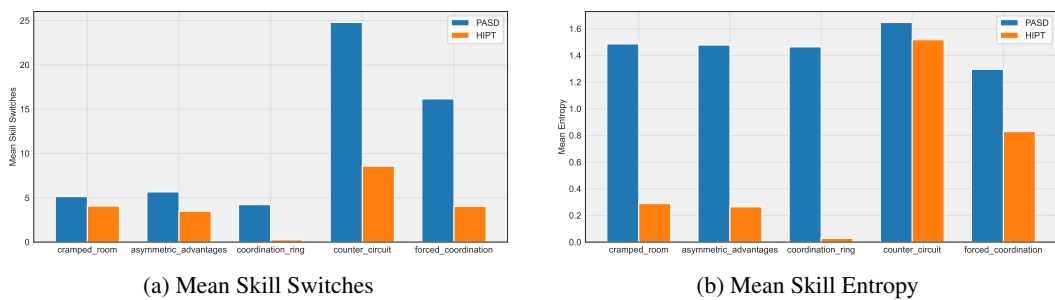
702 **B LAYOUT CHALLENGES AND THE NEED FOR ADAPTIVE SKILL LEARNING**  
703

704 Each Overcooked-AI layout presents unique coordination challenges requiring agents to adapt to  
705 diverse partners with varying skill levels and play styles. In *Cramped Room*, collisions are fre-  
706 quent due to limited space, necessitating adaptable turn-taking and collision avoidance. *Asymmetric*  
707 *Advantages* features partners specializing in different roles, requiring flexible skill activation for  
708 complementary behavior. *Coordination Ring* enforces a looped workflow, demanding alignment  
709 with partners' directional preferences. In *Counter Circuit*, interactions occur via counters, mak-  
710 ing timing and item exchange strategies critical. *Forced Coordination* imposes physical separation,  
711 emphasizing sequenced cooperation and dynamic routines.

712 In addition to the environment reward of +20 for each successful soup delivery, we incorporate  
713 shaped rewards to facilitate effective coordination with diverse partners. Picking up or placing an  
714 onion into a pot yields a small positive reward of +3, while a penalty of -20 is applied when the  
715 partner delivers a soup. These rewards are used in all layouts except *Forced Coordination*, where  
716 strict role asymmetry naturally enforces task specialization. By providing intermediate feedback,  
717 shaped rewards guide the agent to engage in complementary sub-tasks and adapt its behavior to  
718 align with the actions and strategies of different partners, promoting robust collaboration across all  
719 layouts.

720 **C ANALYSIS OF SKILL VARIABILITY AND ADAPTATION ACROSS PARTNERS**  
721

722 We analyze the coordination behavior of PASD and HIPT by quantifying skill usage in terms of  
723 mean skill switches and mean skill entropy across partners (Figure 5). The number of skill switches  
724 captures how frequently an agent changes its skill during an episode, while the entropy measures  
725 the variability in skill selection. Higher switch counts indicate dynamic adaptation to partner ac-  
726 tions, whereas higher entropy reflects diverse skill usage. Across these metrics, PASD consistently  
727 outperforms HIPT. In the first three layouts, skill switches are relatively infrequent, indicating less  
728 heterogeneity in the respective policy pool. The last two layouts show more frequent switches,  
729 reflecting the increased diversity in the partner policy pool, which requires PASD to adapt more  
730 dynamically. Figure 5b shows that entropy remains high across layouts, indicating that PASD ef-  
731 fectively utilizes the full range of available skills rather than collapsing to a few, ensuring that each  
732 skill contributes meaningfully to coordination. In contrast, HIPT demonstrates lower entropy across  
733 layouts, indicating that its skill usage is more collapsed and it relies on a smaller subset of available  
734 skills rather than leveraging the full skill set.



746 Figure 5: Mean skill switches and mean skill entropy across evaluation population pool for PASD  
747 and HIPT across different layouts.

750 **D IMPLEMENTATION DETAILS**  
751

752 We use consistent training settings across all layouts for the PPO objective. Specifically, the entropy  
753 loss coefficient is set to 0.01 for both high- and low-level policies and linearly decays to zero over  
754 the course of training. The value function coefficient is fixed at 0.5, and the PPO clipping coefficient  
755 is set to 0.05. A complete summary of general hyperparameters is provided in Table 4.

756 Certain training parameters, such as the initial learning rate and decay schedule, are tailored to each  
 757 layout to account for differing coordination challenges. Table 5 summarizes these layout-specific  
 758 settings.

760 Table 4: Hyperparameters applied across all layouts.  
 761

762 <b>Hyperparameter</b>	763 <b>Value</b>
764 Entropy coefficient	765 $0.01 \rightarrow 0$ (linear decay)
766 Value function coefficient	767 0.5
768 Clipping coefficient	769 0.05
770 Optimizer	771 Adam
772 Discount factor $\gamma$	773 0.99
774 GAE parameter	775 0.98
776 Batch size	777 64 per environment
778 Parallel environments	779 30

780 Table 5: Layout-specific training parameters. The learning rate decays linearly from the initial value  
 781 to the initial value divided by the decay ratio over training.

782 <b>Layout</b>	783 <b>Initial Learning Rate</b>	784 <b>Decay Ratio</b>
785 Cramped Room	786 $1.0 \times 10^{-3}$	787 3
788 Asymmetric Advantages	789 $1.0 \times 10^{-3}$	790 3
791 Coordination Ring	792 $6.0 \times 10^{-4}$	793 1.5
794 Forced Coordination	795 $8.0 \times 10^{-4}$	796 2
797 Counter Circuit	798 $8.0 \times 10^{-4}$	799 3